Turkish Journal of Electrical Engineering & Computer Sciences

http://journals.tubitak.gov.tr/elektrik/

Research Article

Turk J Elec Eng & Comp Sci
(2016) 24: 2267 – 2273

doi:10.3906/elk-1312-258

An implantable microstrip antenna design for MICS-band biomedical applications

Adnan SONDAŞ*, Mustafa Hikmet Bilgehan UÇAR
Department of Information Systems Engineering, Faculty of Technology, Kocaeli University, İzmit, Kocaeli, Turkey

Received: 30.12.2013 • **Accepted/Published Online:** 08.07.2014 • **Final Version:** 15.04.2016

Abstract: In this paper, an implantable microstrip antenna design is introduced to cover the Medical Implant Communications Service (MICS, 402 – 405 MHz) band for biomedical telemetry systems. The radiating layer of the antenna comprises two concentric square split-ring elements and a metallic pad placed between them. A shorting pin is also used for miniaturization purposes, directly connecting the outer ring element to the ground plane. It is numerically demonstrated that the proposed antenna offers approximately 7% impedance bandwidth and gains of 1.9 dBi at the designated frequency band. In addition, effects of some critical design parameters on the antenna performance are numerically examined in the paper, noting that the full-wave analysis of the implant antenna is carried out using CST Microwave Studio.

Key words: Biomedical telemetry, MICS band, implantable antenna, split-ring elements

1. Introduction

In recent years, considerable progress has been made to develop implantable sensors that can continually monitor the physiological therapies of patients. The implanted sensors must be able to communicate with external devices, thus requiring integrated compact antennas. Designing antennas that would operate in a tissue is an extremely demanding task. Factors such as tissue conductivity, impedance matching, antenna size, low power requirements, and biocompatibility play significant roles in the design [1–8]. For a realistic antenna simulation, the dielectric properties and geometry of the tissue should be taken into consideration. Microstrip patch designs are currently receiving considerable attention for implantable antennas because they are highly flexible in shape and conformability. Meander-shaped dipole elements [1–3], split-ring elements [4], and different types of slot elements [5,6] are used in such designs. A detailed review of the implant antenna designs can be found in [7,8].

Implantable antennas are designed to operate at specific frequency bands, namely the Medical Implant Communications Service (MICS, 402–405 MHz) and/or the Industrial Scientific and Medical (ISM, 2.4–2.48 GHz) [9,10] bands. In this study, we introduce a novel split-ring resonator (SRR)-shaped microstrip antenna design for biomedical telemetry applications in the MICS band. Due to their compact size and inherent properties, SRRs have been preferred in microstrip antenna and filter applications [11–14]. Considering implantable antenna designs in the literature [1–8], the proposed low-loss and low-cost antenna has a compact size of 14 × 14 × 2.54 mm^3 ($\sim 0.02\ \lambda_0 \times 0.02\ \lambda_0$) at 403 MHz, and thus the proposed design can be a good candidate for MICS-band biomedical applications.

The full-wave analysis of the proposed design has been carried out using CST Microwave Studio, utilizing

*Correspondence: asondas@kocaeli.edu.tr

the time-domain finite-integration technique. In this paper, the simulated antenna performance (S_{11}, radiation pattern, electric field distribution, and SAR) is presented. Note that this paper is an extended version of [15], which was previously presented at the ICECCO'2013 conference.

2. Numerical design of the implant antenna

The proposed antenna configuration is depicted in Figure 1. As seen, the radiating layer of the antenna is composed of a pair of concentric square split-ring elements. A metallic pad with a size of 1 × 1 mm is placed between the rings near the outer gap. The separation between the outer and inner ring elements is 1 mm and a coaxial feed is used for excitation. All the metallic elements are sandwiched with substrate/superstrate structure (Rogers RO3210) with a total thickness of $2h = 2.55$ mm, and $\varepsilon_r = 10.2$ ($\tan\delta = 0.003$). A shorting pin directly connects the outer ring element to the ground plane (GP), allowing for miniaturization. In practical implementations, the implantable antenna must be operated in a skin, and thus we modeled the antennas at a depth of 3 mm of a skin ($\varepsilon_r = 31.29$).

The input reflection coefficient (S_{11}) characteristic of the implant antenna is displayed in Figure 2. As can be seen, the proposed antenna provides an approximately 7% impedance bandwidth (389 − 416 MHz) covering the designated MICS band. Note that the $|S_{11}| \leq -10$ dB criterion with 50 Ω system impedance is considered.

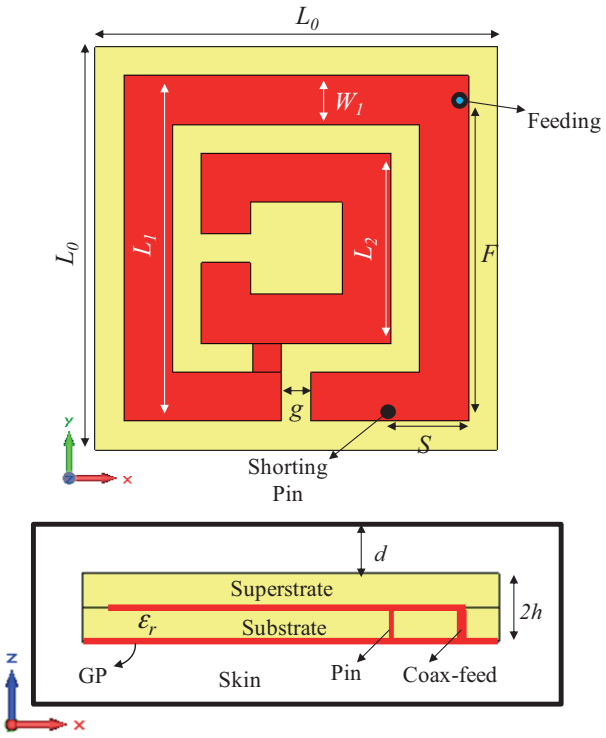

Figure 1. The proposed implantable antenna design: L_0 = 14, L_1 = 12, W_1 = 1.7, g = 1, S = 2.8, F = 11.2, h = 1.27, d = 3 (all in mm), ε_r = 10.2.

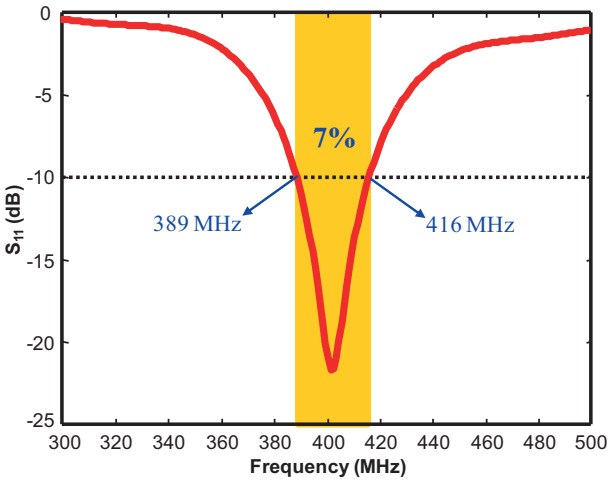

Figure 2. The simulated return loss characteristics of the implantable antenna design.

In designing, the size of the loops, the placement of the metallic pad, and the position of the shorting pin were determined to be critical parameters for achieving the preferred antenna performance in the frequency band of interest. The design steps depicted in Figure 3 have been employed to reach the optimum S_{11}

performance (Figure 2). Figure 4 shows the simulated corresponding frequency response of each design step. First, configuration #1 is constructed by utilizing only a pair of split-ring elements providing a single-band operation centered 1.08 GHz. Second, by employing a shorting pin in an appropriate position that connects the outer ring to the GP (#2), the center of resonance frequency shifts from 1.08 GHz to 578 MHz. Finally, by inclusion of a metallic pad element connecting the outer ring to the inner ring (#3), the projected implantable antenna is achieved and the resonance frequency shifts from 578 MHz to 403 MHz, covering the designated MICS band (402–405 MHz).

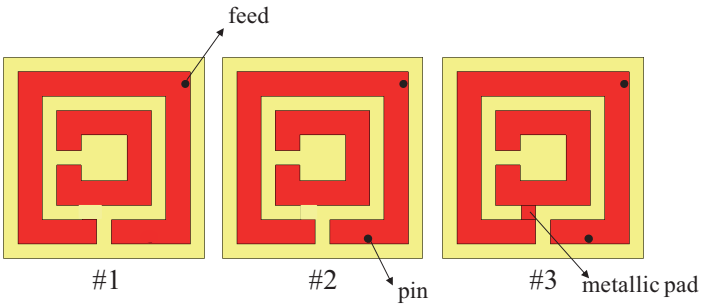

Figure 3. The design steps for the proposed antenna.

In Figure 5, radiation patterns of the proposed antenna at 403 MHz are displayed. As seen, the antenna has a bidirectional radiation pattern in both $\varphi = 0^\circ$ and $\varphi = 90^\circ$ planes. Note that the computed directive gain of the implant antenna design is around 1.9 dBi.

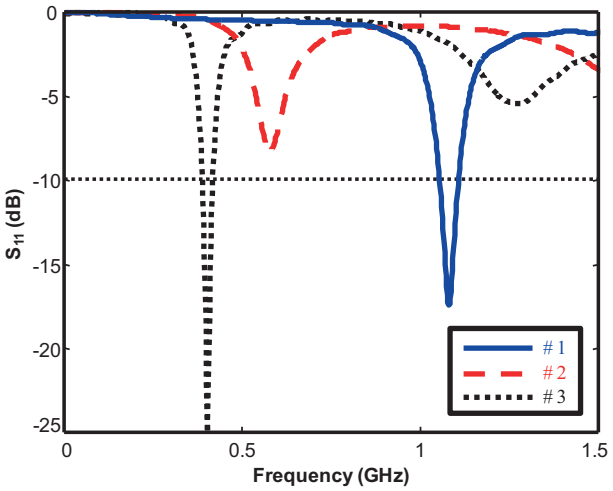

Figure 4. The simulated S11 characteristics of the corresponding design steps #1, #2, and #3 as depicted in Figure 3.

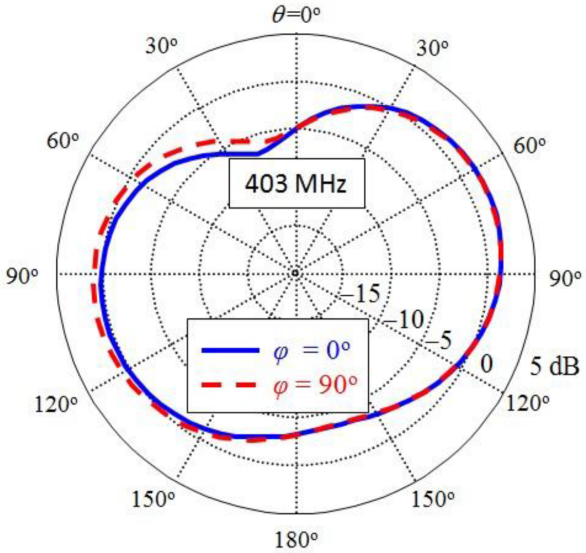

Figure 5. The radiation patterns of the implantable antenna design.

In addition, the computed specific absorption rate (SAR) results have been considered. As shown in Figure 6, a peak 1-g averaged SAR value of 139 W/kg can be obtained, assuming that 1 W is delivered by the proposed antenna. We remark that the delivered power should be decreased to $\leq$11.5 mW to satisfy the practical standard SAR limitation of $\leq$1.6 W/kg [16].

Moreover, the electric field distribution of the proposed implanted antenna at 403 MHz is depicted in Figure 7, where it is observed that the field distribution is mainly concentrated along the ring elements and the metallic pad connecting them, proving the critical role of those elements in the proposed antenna's performance.

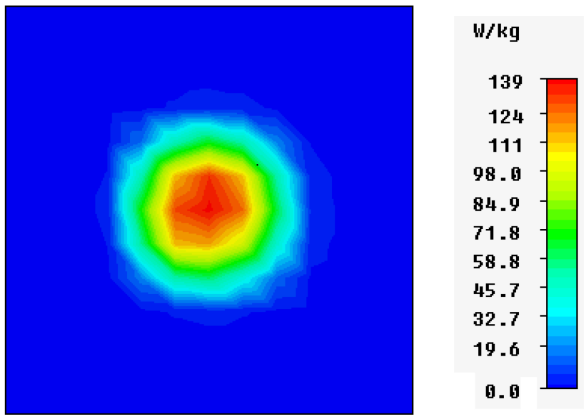

Figure 6. The computed specific absorption rate (SAR) of the implantable antenna design embedded in a simulated part of skin tissue at 403 MHz.

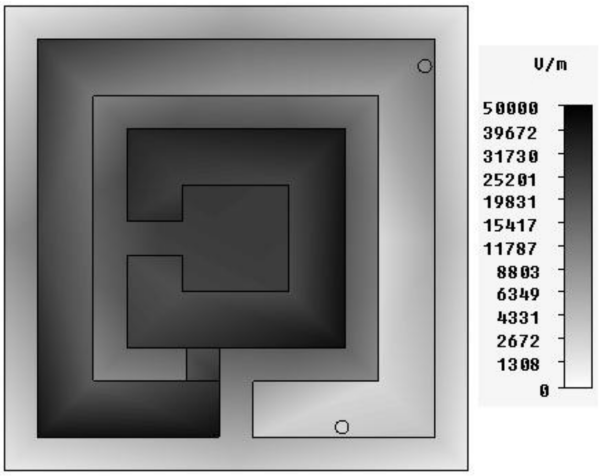

Figure 7. The electric field distribution at 403 MHz.

3. Parametric studies

In order to evaluate the performance of the implantable antenna, a series of parametric studies have been carried out to display the effects of the critical antenna parameters, namely the feed location, the shorting pin location, the metallic pad location, and the inner gap location. Below, we briefly discuss these studies.

3.1. Feed location

The proposed antenna is excited by a standard coaxial probe feed and the location of the feed is expected to change mainly the antenna impedance matching. As can be seen from Figure 8, S_{11} levels change by changing the feed location without any shift in the resonance frequency.

3.2. Shorting pin location

A shorting pin can act as a GP and can reduce the electrical size of the antenna [1] for a given frequency. Hence, by including a shorting pin in the proposed design, the resonance frequency is observed to shift from 738 MHz to 403 MHz (see Figure 9). It is also observed that the pin location not only affects resonance frequency but also affects the antenna matching.

3.3. Metallic pad location

The concentric split-ring elements are connected by a 1 $\times$ 1 mm metallic pad and the location of the pad changes the performance of the antenna. To demonstrate the effects of the pad location, we carried out a series of simulations based on the different pad locations depicted in Figure 10. As can be seen from Figure 11, the pad location affects both the impedance matching and the resonance frequency of the proposed antenna over

the band of 400–580 MHz. For the optimum S_{11} level and maximum miniaturization effect, the #0 location for the metallic pad is selected in the ultimate antenna configuration.

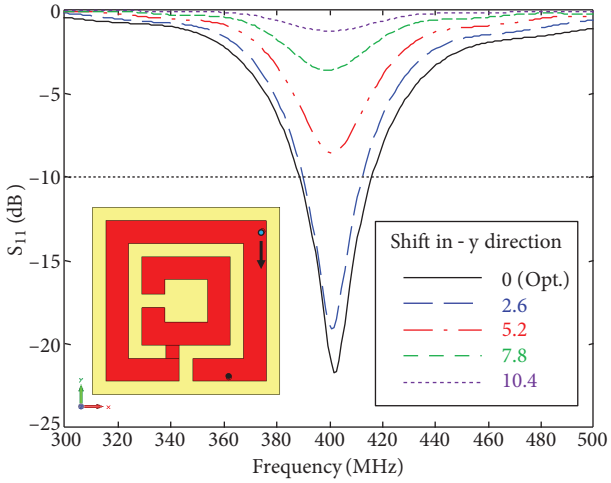

Figure 8. The effects of feed point location on the S_{11} performance.

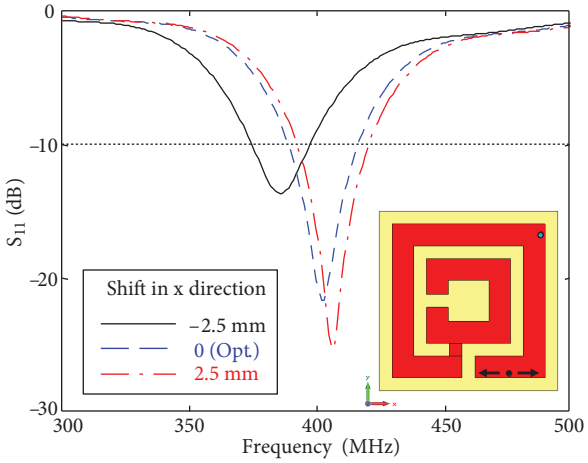

Figure 9. The effects of shorting pin location on the S_{11} performance.

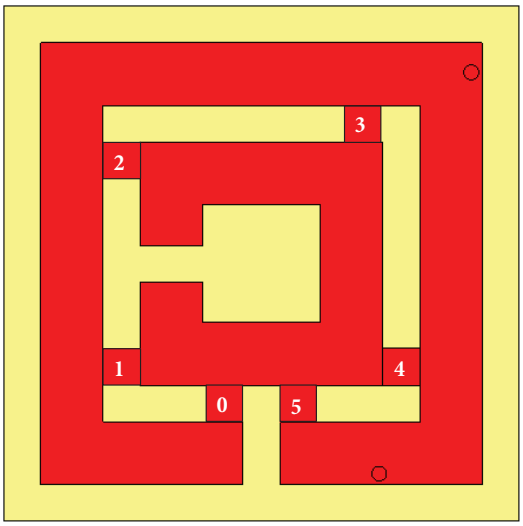

Figure 10. Different metallic pad locations.

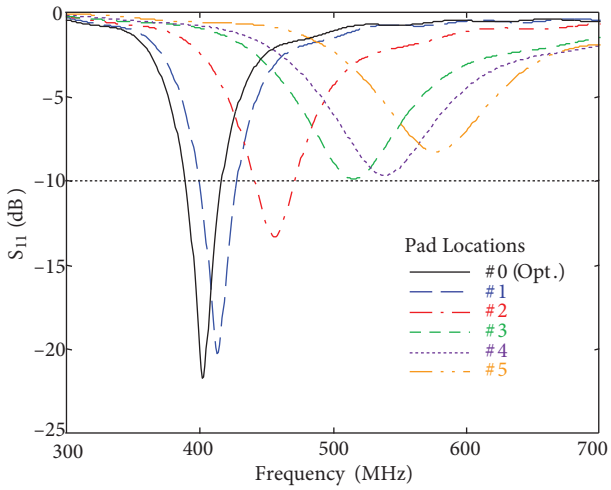

Figure 11. S_{11} performance of the proposed antenna design with respect to different pad locations depicted in Figure 10.

3.4. Inner gap location

The inner square ring element has a size of a 1.7 × 1 mm gap, and the location of this gap may affect the frequency response of the antenna. The S_{11} performances of the proposed antenna design with respect to the different inner gap locations (Figure 12) are depicted in Figure 13. As seen, the inner gap location slightly affects the resonance frequency (max. 10 MHz). Because of the maximum miniaturization effect, the #0 location is

selected in the final antenna configuration. It has also been determined that the inner gap size has a slight effect on the resonance frequency. The optimum design is achieved where the gap size is 1 mm.

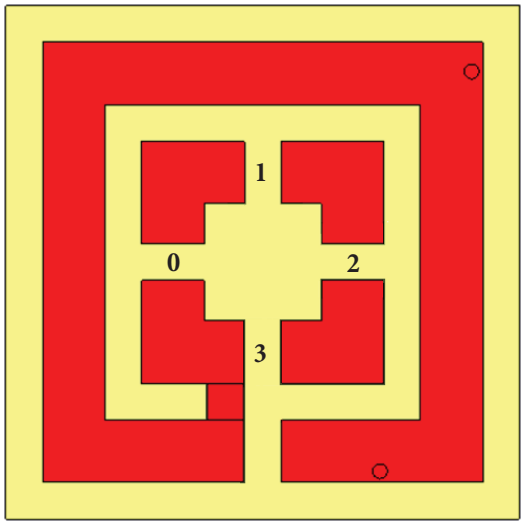

Figure 12. Different inner gap locations.

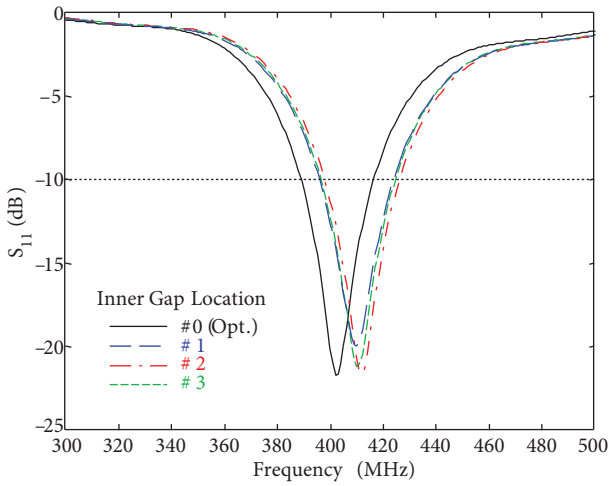

Figure 13. S_{11} performance of the proposed antenna design with respect to different inner gap locations as shown in Figure 12.

4. Conclusions

In this paper, we have introduced a novel implantable antenna design for biomedical telemetry applications in the MICS (402–405 MHz) band. The proposed compact antenna design ($\sim$0.02 λ_0 $\times$ 0.02 λ_0 @ 403 MHz) has a pair of concentric square split-ring elements, a metallic pad, and a shorting pin configuration and is excited by a standard coaxial feed structure. As the shorting pin and the metallic pad play critical roles in the miniaturization of the antenna, the proposed design provides at least 7% impedance bandwidth performance with 1.9 dBi directive gain in the designated frequency band. The effects of some critical design parameters on the antenna performance are also examined. By using a similar antenna configuration, a dual-band performance in the MICS/ISM bands could be obtained.

Acknowledgment

The author would like to thank Dr. Yunus E. Erdemli for his invaluable comments.

References

[1] Soontornpipit P, Furse CM, Chung YC. Design of implantable microstrip antenna for communication with medical implants. IEEE T Microw Theory 2004; 52.8: 1944t1951.

[2] Karacolak T, Hood AZ, Topsakal E. Design of a dual-band implantable antenna and development of skin mimicking gels for continuous glucose monitoring. IEEE T Microw Theory 2008; 56.4: 1001-1008.

[3] Liu WC, Yeh FM, Ghavami M. Miniaturized implantable broadband antenna for biotelemetry communication. Microw Opt Techn Let 2008; 5.9: 2407-2409.

[4] Fernandez CJS, Teruel OQ, Carrion JR, Sanchez LI, Iglesias ER. Dual-band microstrip patch antenna based on short-circuited ring and spiral resonators for implantable medical devices. IET Microw Antenna P 2010; 4: 1048-1055.

[5] Zengin F, Akkaya E, Turetken B, San SE. Design and realization of ultra wide-band implant antenna for biotelemetry systems. In: URSI General Assembly and Scientific Symposium; 13–20 August 2011; İstanbul, Turkey. New York, NY, USA: IEEE. pp. 1-4.

[6] Kiourti A, Costa JR, Fernandes CA, Santiago AG, Nikita KS. Miniature implantable antennas for biomedical telemetry: from simulation to realization. IEEE T Bio-Med Eng 2012; 59: 3140-3147.

[7] Kiourti A, Nikita KS. A review of implantable patch antennas for biomedical telemetry: challenges and solutions. IEEE Antenn Propag M 2012; 54: 210-228.

[8] Topsakal E. Antennas for medical applications: ongoing research and future challenges. In: International Conference on Electromagnetics in Advanced Applications ICEAA'10; 20–24 September 2010; Sydney, Australia. New York, NY, USA: IEEE. pp. 890-893.

[9] Medical Implant Communication Service (MICS) Federal Register. Rules and Regulations 1999; 64: 69926–69934.

[10] European Radiocommunications Commission. Recommendation 70-03 Relating to the Use of Short Range Devices. CEPT/ERC 70-03, Annex 12. Brussels, Belgium: European Radiocommunications Committee, 1997.

[11] IEEE. Special Issue on Metamaterials. IEEE Transactions on Antennas and Propagation, Volume 51. New York, NY, USA: IEEE; 2003.

[12] PIER. Special Issue on Metamaterials Exhibiting Left-Handed Properties and Negative Refraction. Progress in Electromagnetics Research PIER Volume 51. New York, NY, USA: PIER, 2005.

[13] Başaran SC, Erdemli YE. Dual-band split-ring antenna design for WLAN applications. Turk J Electr Eng Co 2008; 16: 79-86.

[14] Ucar MHB, Sondas A, Erdemli YE. Switchable split-ring frequency selective surfaces. Prog Electromagn Res B 2008; 6: 65-79.

[15] Sondas A, Ucar MHB. An implantable microstrip antenna design for biomedical telemetry. In: 10th International Conference on Electronics, Computer and Computation ICECCO'13; 7-9 November 2013; Ankara, Turkey. New York, NY, USA: IEEE. pp. 36-39.

[16] IEEE. Standard for Safety Levels with Respect to Human Exposure to Radiofrequency Electromagnetic Fields, 3 kHz to 300GHz. IEEE Standard C95.1. New York, NY, USA: IEEE, 1999.